Production of hydrogen from methanol over Cu/ZnO and Cu/ZnO/Al_2O_3 catalysts prepared by homogeneous precipitation
- Steam reforming and oxidative steam reforming -

Tetsuya Shishido,[a*] Yoshihiro Yamamoto,[b] Hiroyuki Morioka,[c] and Katsuomi Takehira[b*]

[a] Department of Molecular Engineering, Graduate School of Engineering, Kyoto University, Katsura 1, Nishigyo-ku, Kyoto 615-8510, Japan

[b] Department of Chemistry and Chemical Engineering, Graduate School of Engineering, Hiroshima University, Kagamiyama 1-4-1, Higashi-Hiroshima 739-8527, Japan

[c] Hiroshima Prefectural Institute of Industrial Science and Technology, Kagamiyama 3-10-32, Higashi-Hiroshima 739-8527, Japan.

Received 2006

Corresponding author

T. Shishido

Department of Molecular Engineering, Graduate School of Engineering, Kyoto University, Katsura 1, Nishikyo-ku, Kyoto 615-8510, Japan.

E-mail: shishido@moleng.kyoto-u.ac.jp

Tel.: +81-(0)75-383-2559; FAX: +81-(0)75-383-2561.

K. Takehira

Department of Chemistry and Chemical Engineering, Graduate School of Engineering, Hiroshima University, Kagamiyama 1-4-1, Higashi-Hiroshima 739-8527 Japan.

E-mail: takehira@hiroshima-u.ac.jp

Tel. & Fax.: +81-(0)82-424-6488

Abstract

Two series of Cu/ZnO and Cu/ZnO/Al_2O_3 catalysts with varying Cu/Zn ratio have been prepared by the homogeneous precipitation (*hp*) method using urea hydrolysis. Steam reforming and oxidative steam reforming of methanol were performed using the *hp*-Cu/Zn-based catalysts for catalytic production of hydrogen. The *hp*-Cu/ZnO/Al_2O_3 catalyst showed a higher activity than the *hp*-Cu/ZnO catalysts. In both cases, the catalytic activity was well correlated with the surface area of Cu metal, and the maximum activity was obtained on the *hp*-Cu/ZnO/Al_2O_3 catalyst with the Cu/Zn ratio of 1/1. Although a large amount of Cu^+ was detected on the surface of the Cu/Zn-based catalysts after the reduction at 260 °C, no obvious correlation was observed between the activity and the surface amount of Cu^+. The *hp*-Cu/ZnO/Al_2O_3 catalyst showed a high and stable activity not only for steam reforming but also for oxidative steam reforming of methanol, and the latter reaction effectively produced H_2 with a low CO selectivity at a low temperature around 200 °C. It was confirmed by the temperature-programmed desorption experiments that CH_3OH was first dehydrogenated to HCHO, which then underwent a nucleophilic attack of H_2O to form HCOOH, followed by the decomposition to H_2 and CO_2 on the *hp*-Cu/Zn-based catalysts.

Key Words: Hydrogen production, steam reforming, methanol, Cu/ZnO/Al_2O_3 catalyst, homogeneous precipitation.

1. Introduction

Catalytic steam reforming of methanol is a well-established process used for the production of hydrogen. This process is especially important for polymer electrolyte fuel-cells, which generate electrical power by electrochemical oxidation of hydrogen with atmospheric oxygen [1]. The use of methanol as an on-board hydrogen source is attractive for fuel-cell engines in transportation applications because of its safe handling, low cost and ease of synthesis from a variety of feedstocks (biomass, coal and natural gas) [2]. Moreover, methanol has been recommended as the best source for hydrogen fuel among the high energy density liquid fuels, due to the high H/C ratio having a lower propensity for soot formation than other hydrocarbons, relatively low boiling point and easy storing [3].

Copper-containing catalysts, especially CuZn or CuZnAl mixed oxides, have been the most often studied catalysts in the steam reforming due to their high selectivity and activity [4-9]. It is believed that the active sites in Cu containing catalysts are metallic Cu species [7]. For example, recent *in situ* X-ray diffraction (XRD) and absorption spectroscopy studies showed that the active Cu phase for steam reforming in Cu/ZnO catalysts was completely reduced Cu species [10]. However, the active Cu phase for methanol reforming is not fully elucidated yet. Previously, differences in the reduction kinetics of CuO/ZnO were mainly studied by conventional temperature-programmed reduction (TPR) methods [8,11]. Fierro et al. [11] studied the reduction of CuO/ZnO with different Cu/Zn ratios and found a promoting effect of ZnO on the reducibility of CuO. Structural investigations of the copper phase under reduction conditions based on XRD [12,13] and, moreover, recent time-resolved XANES [14] indicate that Cu_2O

(Cu^+) phase was formed as a transient species in the reduction of Cu^{2+} to Cu^0 although no activity was attributed to it. Only one paper [15] reported Cu_2O as active species in the steam reforming of methanol over CuO/ZrO_2 catalysts. Such formation of Cu^+ species has also been reported in Cu/ZnO catalysts for methanol synthesis [16] and water-gas shift reaction [17,18].

Hydrogen can be obtained directly from methanol according to three different processes: steam reforming (1), partial oxidation (2) and thermal decomposition (3)

$$CH_3OH + H_2O \rightarrow 3H_2 + CO_2 \quad \Delta H^0_{298} = 49.4 \text{ kJ mol}^{-1} \quad (1)$$

$$CH_3OH + 1/2O_2 \rightarrow 2H_2 + CO_2 \quad \Delta H^0_{298} = -192.2 \text{ kJ mol}^{-1} \quad (2)$$

$$CH_3OH \rightarrow 2H_2 + CO \quad \Delta H^0_{298} = 22.4 \text{ kJ mol}^{-1} \quad (3)$$

[9,19-22]. Most fuel-processing technologies reported in the literature so far have been based on either steam reforming (1) or partial oxidation (2); both produce almost quantitatively H_2 and CO_2. While partial oxidation is exothermic, steam reforming is endothermic, and produces a more favorable H_2/CO_2 ratio. Another option is to combine reaction (1) and (2) by co-feeding simultaneously oxygen, steam and methanol through the oxidative methanol reforming. In this process, the heat necessary to maintain steam reforming is supplied by partial oxidation by tuning the ratio of the three reactants as such that the overall reaction heat is nearly neutral.

Mostly $Cu/ZnO/Al_2O_3$ catalysts have been prepared by co-precipitation (*cp*) [7,9,10,11,19,23-28]. Recently the microemulsion method [27], precipitate aging [29] or different pretreatments [28] has been examined to improve the catalytic performance. A few examples have been reported on the use of homogeneous precipitation for the preparation of $Cu/ZnO/Al_2O_3$ catalysts [30-35], although this method generally allows

the preparation of various hydrotalcite-like compounds having a high crystalline degree and a narrow particle-size distribution [36]. In our previous work [34], the results of testing the Cu/ZnO and Cu/ZnO/Al_2O_3 catalysts prepared by homogeneous precipitation (*hp*) in the steam reforming of methanol have been briefly reported. The *hp*-catalysts showed higher activities than those prepared by the *cp*-method. It is suggested that the good catalytic performance of the *hp*-Cu/ZnO and *hp*-Cu/ZnO/Al_2O_3 catalysts is due to both highly dispersed Cu metal species and to high accessibility of the Cu metal species to methanol and steam [34].

In the present paper, we report further details of the activities of the *hp*-Cu/ZnO catalysts, i.e., the effects of the Cu/Zn composition and the Al addition. Moreover, the catalytic behavior of the *hp*-Cu/ZnO catalyst not only in steam reforming but also in autothermal steam reforming of methanol has been discussed in connection with the structure and the kinetic study using temperature programmed desorption.

2. Experimental

2.1. Preparation of the hp-Cu/ZnO and Cu/ZnO/Al_2O_3 catalysts

The Cu/ZnO and Cu/ZnO/Al_2O_3 catalysts with varying metal compositions were prepared by the *hp*-method using urea hydrolysis: urea was mixed into a solution of metal nitrates at room temperature, and the urea was hydrolyzed by heating the mixture to 90 ºC. During the hydrolysis of urea, hydroxide ions are generated in the homogeneous solution (4) and work as the precipitants of metal species. It is expected that the

$$CO(NH_2)_2 + H_2O \rightarrow 2NH_4^+ + HCO_3^- + OH^- \quad (4)$$

homogeneity of the precipitates obtained by this method will be higher than that prepared by the conventional *cp*-method, since there is no gradient in the concentration of precipitants in the solution. The precipitates were then filtered, washed with distilled water, dried at 105 ºC and finally calcined at 300 ºC for 3 h in air. The powders of the mixed oxides obtained were pressed, crushed and sieved to the particles 0.36-0.60 mm in diameter, and used in the reforming reactions.

As controls, several Cu-containing catalysts have been prepared by the *cp*-method. For the *cp*-method, the aqueous solution of metal nitrates was dropped into aqueous solution of Na_2CO_3 with vigorous stirring and the pH was adjusted to 10 with NaOH. The obtained precipitates were dried at 105 ºC, followed by calcination at 300 ºC for 3 h in air. A commercial $Cu/ZnO/Al_2O_3$ catalyst, MDC-7 (Züd Chemie), was also used as a control. MDC-7 as received was first crushed to fine particles, pressed to a disc, crushed roughly and sieved to the particles 0.36-0.60 mm in diameter, and used in the reforming reactions.

The catalysts prepared are designated as *cp*- and *hp*-Cu_a/Zn_b or -$Cu_c/Zn_d/Al_e$ hereafter, in which a/b or c/d/e means the metal composition in the raw materials used for the catalyst preparation.

2.2. Characterization of the catalysts

The structure of the catalysts was studied by using XRD, XPS, AES, SEM, TPR, TPD, ICP, N_2O decomposition and N_2 adsorption.

Powder X-ray diffraction was recorded on a Rigaku powder diffraction unit, RINT

2250VHF, with mono-chromatized Cu *K*α radiation (λ = 0.154 nm) at 40 kV and 300 mA. The diffraction pattern was identified by comparing with those included in the JCPDS (Joint Committee of Powder Diffraction Standards) data base.

X-ray photoelectron spectroscopy (XPS) and Auger electron spectroscopy (AES) were performed with a VG Scientific ESCALAB220i-XL spectrometer by using monochromatic Al Kα and Au mesh as the sample holder. Before measuring the spectra, samples were pre-reduced at 300 ºC for 1 h under the mixed gas flow of H_2/N_2 (1/19 ml min^{-1}). Scanning electron microscope (SEM) measurements were performed with a JEOL JSM-6340F microscope.

Temperature-programmed reduction (TPR) of the catalyst was performed with 50 mg of the catalyst at a heating rate of 10 ºC min^{-1} using a mixture of 5 vol% H_2/Ar (100 ml h^{-1}) as reducing gas. A TCD was used for monitoring the H_2 consumption after passing through a 13X molecular sieve trap to remove water. Prior to the TPR measurements, the sample was treated at 300 ºC for 1.5 h in 20 vol% O_2/ Ar gas (50 ml min^{-1}).

Temperature-programmed desorption (TPD) of CH_3OH or HCHO was carried out to estimate the reaction mechanism of methanol steam reforming on the Cu/Zn-based catalysts. The TPD was performed on a Bell Japan TPD-1-AT equipment in the following manner; 100 mg of a powder sample was heated at a rate of 10 ºC min^{-1} up to 350 ºC and the temperature was kept for 20 min in a gas mixture of H_2/N_2 (5/45 ml min^{-1}) to remove adsorbed molecules and reduce the catalyst surface. The sample was cooled down to 50 ºC in a N_2 (50 ml min^{-1}) gas and evacuated for 5 min. Gaseous CH_3OH was adsorbed at 20 Torr for 10 min and then removed in vacuo for 30 min.

Consecutively, CH_3OH-TPD was started at 50 ºC and the temperature was raised to 600 ºC at a ramping rate of 10 ºC min^{-1} under He gas flow (10 ml min^{-1}-NTP). The products desorbed were determined by using a Q-pole mass spectrometer and recorded on an online personal computer. HCHO-TPD was also carried out in a similar manner using HCHO obtained by thermal decomposition of paraformaldehyde.

Inductively coupled plasma optical emission spectrometry (ICP) was used for the determination of the metal content in each sample synthesized above. The measurements were performed with a Perkin-Elmer OPTIMA 3000 spectrometer, and the sample was dissolved in a mixture of HF and HNO_3 acids before the measurements. The metal compositions obtained by the ICP measurements almost coincided with those calculated from the amount of raw materials in the catalysts preparation.

The copper metal surface areas were determined by the N_2O decomposition method at 90˚C as reported by Evans et al. [37], assuming a reaction stoichiometry of two Cu atoms per oxygen atom and a Cu surface density of 1.63×10^{19} Cu atom m^{-2}. Prior to the measurement, 50 mg of a sample was reduced at 350 ˚C for 1 h in N_2/H_2 (30/5 ml min^{-1}) mixed gas flow.

N_2 adsorption (-196 ºC) study was used to obtain the BET surface area of the mixed oxides. The measurement was carried out on a Micromeritics Flow Sorb II2300 equipment. The samples after the calcination were pretreated in vacuum at 300 ºC for 1 h before the measurements.

2.3. Catalytic reactions and analyses of the products

Steam reforming and oxidative steam reforming were carried out using a fixed

bed reactor at atmospheric pressure. A U-shaped Pyrex glass tube with an inner diameter of 5 mm was used as a reactor. Typically 200 mg of the Cu/Zn-based catalysts in the form of the particles of 0.25-0.42 mmΦ were loaded into the reactor together with 200 mg of quartz beads. A thermocouple was introduced from the top of the reactor, and was placed at the center of the catalyst bed. The catalyst was calcined at 300 ˚C for 1 h and then pre-reduced in a mixed gas flow of H_2/N_2 (5/30 ml min^{-1}) at 350 ˚C for 20 min and finally purged with N_2. The reaction was started by introducing a gas mixture of $CH_3OH/H_2O/N_2$ (10/12/30 ml-NTP min^{-1}) in the steam reforming, while a gas mixture of $CH_3OH/H_2O/O_2/N_2$ (10/12/5/30 ml-NTP min^{-1}) was used in the oxidative steam reforming. N_2 was used as the internal standard for the calculations of the conversions of CH_3OH and H_2O and the yields of products. GHSV was fixed at 6,600 ml g_{cat}^{-1} h^{-1} for the steam reforming, and at 8,100 ml g_{cat}^{-1} h^{-1} for the oxidative steam reforming, and the reaction temperature varied between 150 and 300 ˚C.

The products were analyzed by on-line gas chromatographs (GC). A GC with packed molecular sieves 5A column (3 m × 3 mm i.d.), He carrier gas and TCD were used to analyze N_2, CO, CO_2, CH_4 and other hydrocarbons. Another GC with a packed molecular sieves 5A column (3 m × 3 mm i.d.), Ar carrier gas and TCD were used to analyze H_2 and N_2. CH_3OH, CH_2O, $(CH_3)_2O$ and H_2O were also quantified by another GC with TCD using a packed PEG 20M column (1 m × 3 mm i.d.). All the lines and valves through the water feed, the reactor, the exit and the gas chromatographs were heated to 130 ˚C to prevent the condensation of water.

3. Results and discussion

3.1. Activity of the Cu/Zn-based catalysts for steam reforming of methanol.

The results of steam reforming of methanol over each series of the *hp*-Cu/Zn and the *hp*-Cu/Zn/Al catalysts are shown in Fig. 1 A and B, respectively. In both cases, the activity well correlated with the surface area of Cu metal after the reduction, but not with the BET surface area, suggesting Cu^0 as the active species. The activity of both *hp*-Cu/Zn and *hp*-Cu/Zn/Al catalysts increased with increasing Cu content up to the Cu/(Cu+Zn) atomic ratio of 0.5 (Fig. 1A and B) and the latter showed higher activity than the former. Temperature programmed reduction of the *hp*-Cu/Zn catalysts showed a decrease in the reduction temperature of Cu around the atomic ratio of 0.5 [17], indicating an easy reduction of Cu by the formation of the Cu/Zn binary system. Further increase in the Cu content resulted in a decrease in the activity over the *hp*-Cu/Zn catalysts (Fig. 1A), whereas the activity shown by methanol conversion on the *hp*-Cu/Zn/Al catalysts kept the high value even when the atomic ratio increased above 0.5 (Fig. 1B).

*3.2. Structure of precursors of the Cu/*Zn based *catalysts.*

Typical XRD patterns of the precursors of the *hp*-Cu/Zn and the *hp*-Cu/Zn/Al are shown in Fig. 2 A and B, respectively. In the *hp*-Cu/Zn series, the malachite, $Cu_2(OH)_2CO_3$, phase was formed in the Cu-rich samples and was replaced by the aurichalcite, $(Cu,Zn)_5(OH)_6(CO_3)_2$, phase with increasing Zn content (Figs. 2A a-c). In the *hp*-Cu/Zn/Al series, malachite was obtained as the major component together with hydrotalcite, $(Cu,Zn)_6Al_2(OH)_{16}CO_3{\cdot}4H_2O$, as a concomitant in the Cu-rich samples.

With increasing Zn content, the aurichalcite phase replaced the malachite phase and became a major component (Fig. 2B a-c). In both *hp*-Cu/Zn and *hp*-Cu/Zn/Al series, further increase in the Zn content caused the phase shift from aurichalcite to hydrozincite, $Zn_5(OH)_6(CO_3)_2$ (Fig. 2A c-e and 2B c-e). The mineral aurichalcite (Cu/Zn ratio is 0.67) crystallizes in the monoclinic space group $P2_1/m$ (C^2_{2h}) with lattice parameters: a = 13.82, b = 6.419, c = 5.29 Å and β = 101.04º (Z = 2) [38]. Four crystallographically different Me^{2+} ions exist in the lattice, Me(1) (C_s site symmetry) and Me(2) (C_1 site symmetry) are in tetragonally distorted octahedral sites; Me(3) and Me(4) have tetrahedral and trigonal bipyramidal coordination, respectively (both metal ions are in C_s site symmetry). The three sites Me(1), Me(2), and Me(4) are each occupied by copper and zinc with equal probability, and the tetrahedral site Me(3) is entirely occupied by zinc. On the other hand, the mineral hydrozincite crystallizes in the monoclinic space group $C2/m$ (C^3_{2h}) with lattice parameters: a = 13.62; b = 6.30; c = 5.42 Å and β = 95.83º (Z = 2) [39]. Three different zinc ions exist in the lattice Zn(1) (C_{2h} site symmetry) is coordinated by four oxygen atoms belonging to carbonate ions and by two oxygen atoms from OH^- ions; Zn(2) (C_2 site symmetry) is coordinated by four oxygen atoms from OH^- ions and two oxygen atoms from carbonate ions; Zn(3) (C_s site symmetry) is tetrahedrally coordinated by three oxygen atoms from OH^- ions and one oxygen atom from the carbonate ions. Natural and synthetic aurichalcites are known with Cu/Zn ratios in the range of 0.2-1 [40,41], whereas synthetic hydrozincite forms solid solution $(Cu_xZn_{1-x})_5(OH)_6(CO_3)_2$ (x = 0-0.3) [42]; phase shift from aurichalcite to hydrozincite seems to take place continuously by replacing the Cu sites with Zn [38,39,43].

It was reported that the presence of Cu^{2+} cations makes the synthetic procedures of pure hydrotalcite more complex by conventional urea hydrolysis procedure [31,32], at least for two reasons. First, Cu^{2+} ions show the Jahn-Teller effect that favors the formation of distorted octahedral structures. As a result, the insertion of Cu^{2+} ions into the brucite-like sheet is unfavored, and preferentially gives rise to the precipitation of the malachite phases. Secondarily, Cu^{2+} ions can be depleted by ammonia originated from urea hydrolysis. The first issue was confirmed in the present work by the preferential formation of the malachite phase. However the second point was not so detrimental in the present work, since the metal compositions determined after the calcination were almost same as those in the raw materials used in the preparation [17,18]. Moreover, it has been found [44] that the presence of other divalent cations, such as Mg^{2+}, Zn^{2+} and Co^{2+}, favors the accommodation of Cu^{2+} into the sheet, giving rise to ternary hydrotalcite phases.

The line intensity of aurichalcite (Fig. 2) well correlates to the catalytic activity shown as CH_3OH conversion (Fig. 1), from the view point of their dependence on the Cu/Zn composition. It is suggested that the formation of aurichalcite in the catalyst precursor brings about a positive effect on the activity of the Cu/Zn-based catalysts finally obtained, although many phases were produced in both series of catalyst precursors. Aurichalcite possesses closely located Cu and Zn ions which are bridged by oxygen atoms each; such crystal structure results in the formation of highly dispersed CuO and ZnO particles which are strongly interacted with each other after the calcination and finally form highly dispersed Cu metal particles after the reduction (*vide infra*).

3.3. Morphology of precursors of the Cu/Zn-based catalysts.

SEM observation of the precursors of the *hp*-Cu_{50}/Zn_{50} catalyst clearly showed the formation of spherical fine particles (ca. 10 μm in diameter) in the magnifications of ×500 and ×8,500 (Fig. 3a and b). Spherical fine particle seems to be assembly of thin plate-like structures and the surface is not smooth in the magnification of ×20,000 (Fig. 3c). Spherical fine particles were evidently observed for the samples showing the strong reflection of aurichalcite in the XRD (Fig. 2). Such spherical fine particle structure with high surface area was maintained even after the calcination at 300 ºC for 3 h in air, and is supposed to possess an important role in the catalytic activity. When the Cu content was increased up to 80 mol % (*hp*-Cu_{80}/Zn_{20}), some aggregates of fine particle were observed with both symmetry and sphericalness lost as seen in the magnification of ×2,500 (Fig. 3d). This phenomenon well correlates with the low activity of *hp*-Cu_{80}/Zn_{20} compared with that of *hp*-Cu_{50}/Zn_{50} shown in Fig. 1A.

3.4. Particle size of Cu metal on the Cu/Zn-based catalysts.

In the XRD patterns of the precursors of both *hp*-Cu/Zn and *hp*-Cu/Zn/Al samples after the precipitation, various phases were observed together with aurichalcite depending on the compositions (Fig. 2A and B). After the calcination at 300 ºC for 3 h in air, all these phases disappeared in the XRD patterns and the reflection lines of both CuO and ZnO appeared for all Cu/Zn-based catalysts with varying intensities depending on the metal compositions and the preparation methods (data are not shown). After the reduction treatment, the lines of CuO were replaced by those of Cu metal.

Particle sizes of CuO and ZnO after the calcination, Cu metal and ZnO after the reduction and those after the reaction were calculated from the line width in the XRD using Scherrer equation and are shown in Table 1. Before the reaction the particle size of CuO could not be precisely determined for either *hp*-Cu_{50}/Zn_{50} or *hp*-$Cu_{45}/Zn_{45}/Al_{10}$ samples, since the CuO lines were too much broadened and feeble. The sizes of ZnO particles were also small for both *hp*-Cu_{50}/Zn_{50} and *hp*-$Cu_{45}/Zn_{45}/Al_{10}$ samples. After the reduction at 350 ºC, the sizes of the particles of both Cu metal and ZnO increased for both *hp*-Cu_{50}/Zn_{50} and *hp*-$Cu_{45}/Zn_{45}/Al_{10}$ samples, but still maintained the smallest values among the catalysts tested (Table 1). The addition of Al_2O_3 was obviously effective for suppressing the size growth of the particles of CuO, Cu metal and ZnO for the *hp*-Cu/Zn-based catalysts. After the reaction between 200 and 300 ºC, particle sizes of both Cu metal and ZnO slightly increased. Increase in the Cu metal particle size was rather significant for the *cp*-catalysts compared to the *hp*-catalysts.

Particle sizes of Cu metal and ZnO for both *hp*-Cu/Zn and *hp*-Cu/Zn/Al catalysts after the reactions are shown in Fig. 4. The size of Cu metal increased with increasing Cu content, while that of ZnO kept almost constant values irrespective of the Cu content. Increase in the Cu metal particle size resulted in a decrease in the Cu^0 surface area which in turn caused a decrease in the activity (Fig. 1). The sizes of both Cu metal and ZnO particles were smaller on the *hp*-Cu/Zn/Al than on the *hp*-Cu/Zn catalysts, leading to higher activity of the *hp*-Cu/Zn/Al catalysts than the *hp*-Cu/Zn catalysts (Fig. 1). This is well explained by the effect of Al_2O_3 addition as suggested above, although the precise role of Al_2O_3 cannot be well elucidated since no positive evidence is obtained from the structure analyses by XRD (Fig. 2) and TPR [17].

3.5. Formation of Cu^+ species on the hp-Cu/Zn-based catalysts.

In the precursors of the *hp*-Cu/Zn and the *hp*-Cu/Zn/Al catalysts prepared by urea hydrolysis, various phases, i.e. malachite, aurichalcite, hydrozincite, hydrotalcite and $Zn_4(OH)_6CO_3 \cdot H_2O$, were formed. It is likely that aurichalcite among these phases substantially affects the structure after the calcination leading to the high activity of the *hp*-Cu/Zn-based catalyst finally obtained by the reduction.

We reported on Auger-electron spectra of the *hp*-Cu/Zn and *hp*-Cu/Zn/Al catalysts after the reduction in the previous paper [17]. According to the results reported by Batsita et al. [45], Cu^0 and Cu^+ species have the following values of the kinetic energy (Cu-LMM): 918.6 eV and 916.5 eV, respectively. A peak assigned to Cu^+ was clearly observed at 917.0 eV together with that of Cu^0 at 919.0 eV in the Cu-LMM Auger spectrum of *hp*-Cu/Zn catalysts not only after the reduction but also after the reaction and their intensities varied depending on the Cu/Zn ratio. Moreover a satellite peak characteristic of Cu^{2+} was unobservable around 945 eV in the XPS of Cu 2p3/2 on the *hp*-Cu/Zn samples both after the reduction and after the reaction (data are not shown) [46]; thus, the oxidation state of Cu could be zero- or mono-valent. It is therefore concluded that Cu^+ species was formed on *hp*-Cu/Zn catalysts both after the reduction and after the reaction.

As reported in the previous paper [17], Auger peaks were more intensive for the *hp*-Cu/Zn than for *hp*-Cu/Zn/Al; these catalysts were pre-reduced at 300 °C for 1 h. The peak area of Cu^+ and Cu^0 in the Auger spectra was estimated after the deconvolution and the value of $Cu^+/(Cu^+ + Cu^0)$ peak area % was calculated from each peak area (data

are not shown). The amount of Cu^+ obviously increased, reached the maximum value at the Cu/(Cu+Zn) atomic ratio of 0.5, and decreased with further increase in the Cu content. For the *hp*-Cu/Zn/Al catalysts, the amount of Cu^+ increased with increasing Cu content, reached the maximum value, and then kept almost constant values with further increase in Cu content. These apparently coincided with the dependence of the activity shown as the conversion of methanol on the Cu content for each series of the catalysts (Fig. 1A and B). However, the amount of Cu^+ was definitely larger on the *hp*-Cu/Zn catalysts than on the *hp*-Cu/Zn/Al catalysts [17] contrarily to the order of the activity of these catalysts. After the reaction, the Cu^+ amount decreased for the samples of the Cu/(Cu+Zn) atomic ratio around 0.5, while those increased for the samples of high Cu content, suggesting that the catalyst have been altered during the reaction.

In the present work, no obvious correlation was observed between the amount of Cu^+ and the catalytic activity; the direct contribution of Cu^+ species to the activity can be therefore neglected. It is considered highly dispersed Cu metal species formed accompanied by the formation of Cu^+ species due to interface interaction between Cu and ZnO on the *hp*-Cu/Zn-based catalysts, and the real active species for the steam reforming of methanol must be Cu metal.

3.6. Oxidative steam reforming of methanol over the hp-Cu/Zn-based catalysts.

The effect of the addition of oxygen in the feed gas of methanol steam reforming is shown in Fig. 5. Stoichiometric amount of oxygen, i.e., O_2/CH_3OH = 1/2, for completing the partial oxidation (2) was present in the feed gas. By the addition of oxygen, the conversion of methanol increased at low temperatures with the low

selectivity to CO still kept. It was reported that CH_2O, $(CH_3)_2O$ and CH_4 were produced as the by-products together with H_2, CO_2 and CO at all temperatures in the oxidative steam reforming of methanol ($CH_3OH/H_2O/O_2$ = 10/11/1.2) over the $Cu/ZnO/Al_2O_3$ (Cu/Zn/Al = 18/33/49) catalyst derived from hydrotalcite precursors [33]. However, none of CH_2O, $(CH_3)_2O$ and CH_4 was produced in the present reaction over both *hp*-Cu/Zn and *hp*-Cu/Zn/Al catalysts.

Time course of the oxidative steam reforming reaction for 25 h over *hp*-$Cu_{45}/Zn_{45}/Al_{10}$, *hp*-Cu_{50}/Zn_{50}, and *cp*-Cu_{50}/Zn_{50} together with a commercial $Cu/ZnO/Al_2O_3$ catalyst are shown in Fig. 6. The *hp*-$Cu_{45}/Zn_{45}/Al_{10}$ catalyst showed high and stable activity, followed by the commercial $Cu/ZnO/Al_2O_3$ catalyst. The *hp*-Cu_{50}/Zn_{50} catalyst showed activity and sustainability almost similar to the commercial $Cu/ZnO/Al_2O_3$ catalyst as well as higher activity than the *cp*-Cu_{50}/Zn_{50} catalyst, indicating the superiority of the *hp*-preparation. The selectivity to CO was always less than 1.0 % over all catalysts tested. The *hp*-Cu_{50}/Zn_{50} catalyst showed CO selectivity almost similar to that of the *cp*-Cu_{50}/Zn_{50} catalyst, although the activity was far higher on the former than on the latter. Moreover, the CO selectivity gradually decreased during the reaction over the *hp*-Cu_{45}/Zn_{45}/Al catalyst, although no decline in the CH_3OH conversion was observed, suggesting that the catalyst surface was improved by the Al_2O_3 addition to suppress the CO formation.

3.7. Mechanism of steam reforming of methanol over the hp-Cu/Zn-based catalysts.

The results of CH_3OH-TPD on the *hp*-Cu/Zn/Al catalysts are shown in Fig. 7. Desorptions of HCHO and then H_2 from CH_3OH were observed at 120-140 ºC and

160-180 ºC, respectively, indicating that CH_3OH was dehydrogenated to HCHO around 130 ºC, and H_2 after the recombination of H atoms was desorbed at slightly higher temperature around 170 ºC over the *hp*-Cu/Zn/Al catalysts. Judging from the findings shown in Fig. 1 and the discussions in the preceding section, the active site for the CH_3OH dehydrogenation is likely to be Cu metal. The desorptions of both H_2 and HCHO were enhanced with increase in the Zn content, i.e., the Cu^0 surface area, reached the maximum around 1/1 of the Cu/Zn ratio. Further increase in the Zn content resulted in an increase in the desorption temperature where Cu^0 surface area decreased (Fig. 1); HCHO peak showed no significant decrease while H_2 peak decreased, suggesting that the selectivity to both H_2 and CO_2 decreased. Actually the rate of H_2 production decreased over the Zn-rich catalysts although CH_3OH conversion kept high value (Fig. 1) and the maximum rate of H_2 production was observed over the *hp*-$Cu_{45}/Zn_{45}/Al_{10}$ catalyst.

The results of HCHO-TPD on the *hp*-Cu/Zn catalysts are shown in Fig. 8. The desorption peaks of both CO_2 and H_2 appeared around 150 ºC mostly over the *hp*-Cu/Zn catalysts containing Cu. Both CO and H_2O desorbed also around 150 ºC although their intensities were very weak. The second desorption peaks appeared around 300 ºC for all H_2, CO_2, CO and H_2O over the Zn-rich catalysts. On the other hand, the desorptions of H_2, CO_2 and CO appeared around a little higher temperature on the *hp*-Cu/Zn/Al catalysts (data are not shown) than on the *hp*-Cu/Zn catalysts. Moreover, the desorption of H_2 appeared around a little higher temperature, i.e., 180 ºC, than that of CO_2 around 160 ºC over the *hp*-Cu/Zn/Al catalysts.

There has been limited amount of published research that provides information

specifically concerning the reaction scheme for methanol steam reforming on the $Cu/ZnO/Al_2O_3$ catalyst. In the study using a $Cu/ZnO/Al_2O_3$ catalyst containing only labeled oxygen (^{18}O), upon addition of unlabeled methanol and steam, doubly labeled carbon dioxide ($C^{18}O^{18}O$) was immediately detected in the product stream and its proportion increased to a maximum at which point 90 % of the carbon dioxide produced was doubly labeled [47]. $C^{18}O$, however, was never detected in the product stream, indicating that the CO bond in methanol is not broken in the mechanism of decomposition. These results indicate that there is a separate path for the CO producing reaction that does not involve oxygen interchange with the catalyst unlike the CO_2 producing reaction.

Methanol was adsorbed on a partially oxidized $Cu/ZnO/Al_2O_3$ catalyst at room temperature, followed by temperature programmed decomposition [48]; the reaction spectrum of the products obtained using a mass spectrometer showed that CO_2 and H_2 were produced simultaneously at 167 ºC. From previous experiments this peak could be assigned to the decomposition of an adsorbed formate species on copper sites. At 307 ºC, CO and H_2 were simultaneously evolved, being attributed to the decomposition of a formate species on ZnO.

Judging from the results of CH_3OH-TPD (Fig. 7), it is considered that CH_3OH is dehydrogenated to form HCHO and H_2 on Cu metal as the first step of steam reforming of methanol. HCHO is then converted to $HCOOCH_3$ by the nucleophilic attack of CH_3OH under the steam reforming reaction conditions [6]. The desorption spectrum from HCHO obtained for the *hp*-Cu/Zn catalysts in the present work (Fig. 8) almost coincided with the reaction spectrum obtained by temperature programmed

decomposition of methanol [48]. As a consequence, the reaction scheme is proposed as shown in Scheme 1: CH_3OH is dehydrogenated to HCHO, HCHO is followed by nucleophilic attack of H_2O to form HCOOH, which in turn decomposed to H_2 and CO_2 on the *hp*-Cu/Zn-based catalysts [9]. It is concluded that both CO_2 and H_2 desorbed around 150 ºC in the HCHO-TPD profile are derived from the decomposition of HCOOH on Cu metal, whereas CO desorbed around 300 ºC is due to the decomposition of HCOOH on ZnO. Small deviations of the peak temperatures observed in the HCHO-TPD over the *hp*-Cu/Zn/Al catalysts are probably due to the contribution of Al_2O_3 on the catalytic activity, i.e., the formation of acid site, etc. The formation of small amount of CO is probably due to the reverse water-gas shift reaction (5) on Cu

$$CO_2 + H_2 \rightarrow H_2O + CO \qquad \Delta H^0_{298} = 41.0 \text{ kJ mol}^{-1} \qquad (5)$$

metal, since almost the same amount of H_2O as that of CO was produced at 150-160 ºC, indicating a separate path for the CO producing reaction.

4. Conclusions

The homogeneous precipitation (*hp*) method has been comparatively examined in the preparation of the Cu/Zn-based catalysts with the co-precipitation (*cp*) method. Both *hp*-Cu/ZnO and *hp*-Cu/ZnO/Al_2O_3 catalysts with varying Cu/Zn ratios have been prepared using urea hydrolysis. Steam reforming and oxidative steam reforming of methanol were performed using the Cu/Zn-based catalysts for catalytic production of hydrogen. The *hp*-Cu/ZnO/Al_2O_3 catalyst showed higher activity than the *hp*-Cu/ZnO catalysts, and the maximum activity was obtained on the *hp*-Cu/ZnO/Al_2O_3 catalyst

with the Cu/Zn ratio of 1/1. The catalytic activity was well correlated with the surface area of Cu^0 but not with the surface amount of Cu^+, although a large amount of Cu^+ was detected on the surface of the Cu/Zn-based catalysts after the reduction. It seems that the aurichalcite phase substantially contributes to the activity of the Cu/Zn-based catalyst by forming finely dispersed Cu metal particles after the reduction. The *hp*-Cu/ZnO/Al_2O_3 catalyst showed a high and stable activity not only for steam reforming but also for oxidative steam reforming of methanol, the latter of which effectively produced H_2 with a low CO selectivity at a low temperature. According to the results of the temperature-programmed desorption experiments, it was confirmed that CH_3OH was dehydrogenated to HCHO followed by a nucleophilic attack of H_2O to form HCOOH, which in turn decomposed to H_2 and CO_2 on the *hp*-Cu/Zn-based catalysts.

References

[1] P.J. de Wild, M.J.F.M. Verhaak, Catal. Today 60 (2000) 3.

[2] P. Kluger, Int. J. Hydrogen Energy 26 (2001) 1137.

[3] J.O.M. Bockris, Int. J. Hydrogen Energy 24 (1999) 1.

[4] H. Kobayashi, N. Takezawa, C. Minochi, J. Catal. 69 (1981) 487.

[5] R.O. Idem, N.N. Bakhshi, Ind. Eng. Chem. Res. 34 (1995) 1548.

[6] N. Takezawa, N. Iwasa, Catal. Today 36 (1997) 45.

[7] G.-C. Shen, S.-I. Fujita, S. Matsumoto, N. Takezawa, J. Mol. Catal. A 124 (1997) 123.

[8] J.P. Breen, J.R.H. Ross, Catal. Today 51 (1999) 521.

[9] B.A. Reppley, J.C. Amphlett, L.M. Kearns, R.F. Mann, Appl.Catal. A 179 (1999) 21.

[10] M.M. Günter, T. Ressler, R.E. Jentoft, B. Bems, J. Catal. 203 (2001) 133.

[11] G. Fierro, M. Lo Jacono, M. Inversi, P. Porta, F. Cioci, R. Lavecchia, Appl. Catal. A 137 (1996) 327.

[12] P.B. Himelfarb, F.E. Wagner, Jr., A. Bieser, Jr., S.N. Vines, J. Catal. 83 (1983) 469.

[13] P. Porta, R. Dragone, M. Lo Jacono, G. Minelli, G. Moretti, Solid State Ionics, 32/33 (1989) 1019.

[14] T.L. Reitz, P.L. Lee, K.F. Czaplewski, J.C. Lang, K.E. Popp, H.H. Kung, J. Catal. 199 (2001) 193.

[15] H. Oguchi, H. Kanai, K. Utani, Y. Matsumuira, S. Imamura, Appl. Catal. A 293 (2005) 64.

[16] T. Fujitani, J. Nakamura, Appl. Catal. A 191 (2000) 111.

[17] T. Shishido, M. Yamamoto, D. Li, Y. Tian, H. Morioka, M. Honda, K. Takaki, K. Takehira, Appl. Catal. A 303 (2006) 62.

[18] T. Shishido, M. Yamamoto, I. Atake, D. Li, Y. Tian, H. Morioka, M. Honda, T. Sano, K. Takehira, J. Mol. Catal. A 253 (2006) 270.

[19] J. Agrell, M. Boutonnet, J.L.G. Fierro, Appl. Catal. A 253 (2003) 213.

[20] R. Peters, H.G. Düsterwald, B. Höhlein, J. Power Sources 86 (2000) 507.

[21] R. Shiozaki, T. Hayakawa, T. Ishii, M. Kumagai, S. Hamakawa, K. Suzuki, T. Ito, T. Shishido, K. Takehira, Catal. Lett. 58 (1999) 131.

[22] T. Shishido, H. Sameshima, K. Takehira, Topics Catal. 22 (2003) 279.

[23] F.S. Stone, D. Waller, Topics Catal. 22 (2003) 305.

[24] B.A. Reppley, J.C. Amphlett, L.M. Kearns, R.F. Mann, Appl.Catal. A 179 (1999) 31.

[25] J.-P. Shen, C. Song, Catal. Today 77 (2002) 89.

[26] S.R. Segel, K.B. Anderson, K.A. Carrado, C.L. Marshall, Appl. Catal. A 231 (2002) 215.

[27] J. Agrell, M. Boutonnet, I. Melián-Cabrera, J.L.G. Fierro, Appl. Catal. A 253 (2003) 201.

[28] P.H. Matter, D.J. Braden, U.S. Ozkan, J. Catal. 223 (2004) 340.

[29] B.L. Kniep, F. Girgsdies, T. Ressler, J. Catal. 236 (2005) 34.

[30] J. Agrell, K. Hasselbo, K. Jansson, S.G. Järås, M. Boutonnet, Appl. Catal. A 211 (2001) 239.

[31] S. Murcia-Mascarós, R.M. Navarro, L. Gómez-Sainero, U. Constantino, M.

Nocchetti, J.L.G. Fierro, J. Catal. 198 (2001) 338.

[32] M. Turco, G. Bagnasco, U. Constantino, F. Marmottini, T. Montanari, G. Ramis, G. Busca, J. Catal. 228 (2004) 43.

[33] M. Turco, G. Bagnasco, U. Constantino, F. Marmottini, T. Montanari, G. Ramis, G. Busca, J. Catal. 228 (2004) 56.

[34] T. Shishido, Y. Yamamoto, H. Morioka, K. Takaki, K. Takehira, Appl. Catal. A 263 (2004) 249.

[35] U. Constantino, F. Marmottini, M. Sisani, T. Montanari, G. Ramis, G. Busca, M. Turco, G. Bagnasco, Solid State Ionics, 176 (2005) 2917.

[36] U. Contantino, F. Marmottini, M. Nocchetti, R. Vivani, Eur. J. Inorg. Chem. (1998) 1439.

[37] J.W. Evans, M.S. Wainwright, A.J. Bridgewater, D.J. Young, Appl. Catal. 7 (1983) 75.

[38] M.H. Marjorie, B.M. Kariuki, Acta Crystallogr. B 50 (1994) 673.

[39] S. Ghose, Acta Crystallogr. 17 (1964) 1051.

[40] J.L. Jambor, Acta. Crystallogr. 17 (1964) 1051.

[41] J.W. Couves, J.M. Thomas, D. Waller, R.H. Jones, A.J. Dent, G.E. Derbyshire, G.N. Greaves, Nature 354 (1991) 465.

[42] R.T. Figueiredo, A.L.D. Ramos, H.M. Carvalho de Andrade, J.L.G. Fierro, Catal. Today 107-108 (2005) 671.

[43] D. Stoilova, V. Koleva, V. Vassileva, Spectrochimica Acta A 58 (2002) 2051.

[44] F. Cavani, F. Trifirò, A. Vaccari, Catal. Today 11 (1991) 173.

[45] J. Batista, A. Pintar, D. Mandrino, M. Jenko, V. Martin, Appl. Catal. A 206 (2001)

113.

[46] Y. Tanaka, R. Kikuchi, T. Takeguchi, K. Eguchi, Appl. Catal. B 57 (2005) 211.

[47] N.E. Vanderborgh, B.E. Goodby, T.E. Springer, Proceed. 32nd Int. Power Sources Symp. 1986, pp. 623.

[48] K.C. Waugh, Catal. Today 15 (1992) 51.

Table 1. Particle sizes[a)] of CuO, Cu^0 and ZnO of the Cu/Zn-based catalysts after the calcination (A), after the reduction (B) and after the reaction (C).[b)]

Catalyst	A / nm		B / nm		C / nm	
	CuO	ZnO	Cu^0	ZnO	Cu^0	ZnO
cp-Cu_{50}/Zn_{50}	17.6	31.0	24.8	27.3	29.2	33.7
cp-$Cu_{45}/Zn_{45}/Al_{10}$	26.5	24.7	28.2	31.5	30.1	32.5
hp-Cu_{50}/Zn_{50}	n.d.	9.8	12.5	13.0	13.1	13.7
hp-$Cu_{45}/Zn_{45}/Al_{10}$	n.d.	8.5	11.0	12.5	11.5	13.0

a) Determined by XRD from the half-width of the main Ni peaks.

b) The catalyst was calcined at 300 ºC for 1 h and pre-reduced at 350 ºC with a H_2/N_2 (5/30 ml min^{-1}) for 20 min and used in the reaction under the following conditions: catalyst, 200 mg (+ quartz beads 200 mg); $CH_3OH/H_2O/N_2$ = 10/12/30 ml-NTP min^{-1}; reaction time: 1 h for each reaction temperature of 200 ºC, 250 ºC and 300 ºC.

Figure captions

Fig. 1 CH_3OH steam reforming over the *hp*-Cu/Zn (A) and *hp*-Cu/Zn/Al (B) catalysts.

$CH_3OH/H_2O/N_2$ = 10/12/30 ml min^{-1}; catalysts, 200 mg; pre-reduced with H_2/N_2 (5/30 ml min^{-1}) at 350 °C for 20 min.

●, CH_3OH conversion (──, 250 °C; -----, 200 °C); □, BET surface area; ○, Cu^0 surface area.

Fig. 2 XRD patterns of the precursors of the *hp*-Cu/Zn (A) and *hp*-Cu/Zn/Al (B) catalysts after the precipitation.

(A): a) *hp*-Cu_{90}/Zn_{10}; b) *hp*-Cu_{70}/Zn_{30}; c) *hp*-Cu_{50}/Zn_{50}; d) *hp*-Cu_{30}/Zn_{70}; e) *hp*-Cu_{10}/Zn_{90}.

(B) : a) *hp*-$Cu_{80}/Zn_{10}/Al_{10}$; b) *hp*-$Cu_{60}/Zn_{30}/Al_{10}$; c) *hp*-$Cu_{45}/Zn_{45}/Al_{10}$; d) *hp*-$Cu_{30}/Zn_{60}/Al_{10}$; e) *hp*-$Cu_{10}/Zn_{80}/Al_{10}$.

●, $(Cu,Zn)_5(CO_3)_2(OH)_6$: aurichalcite; □, $Zn_5(CO_3)_2(OH)_6$: hydrozincite; ○, $Cu_2CO_3(OH)_2$: malachite; ▲, $Zn_4CO_3(OH)_6{\cdot}H_2O$; ■, $(Cu,Zn)_6Al_2(OH)_{16}CO_3{\cdot}4H_2O$: hydrotalcite

Fig. 3 SEM images of the *hp*-Cu_{30}/Zn_{70} and *hp*-Cu_{80}/Zn_{20} catalysts.

Catalysts and magnifications: a) *hp*-Cu_{50}/Zn_{50} ×500; b) *hp*-Cu_{50}/Zn_{50} ×8,500; c) *hp*-Cu_{50}/Zn_{50} ×20,000; d) *hp*-Cu_{80}/Zn_{20} ×2,500.

Fig. 4 Particle sizes of Cu^0 and ZnO in the *hp*-Cu/Zn and *hp*-Cu/Zn/Al catalysts after the reactions.

●, Cu^0 in *hp*-Cu/Zn; ○, Cu^0 in *hp*-Cu/Zn/Al; ■, ZnO in *hp*-Cu/Zn; □, ZnO in

hp-Cu/Zn/Al.

Fig. 5 Effect of the addition of O_2 in the steam reforming of CH_3OH over the *hp*-Cu_{50}/Zn_{50} catalyst.

Catalyst, 0.2 g; $CH_3OH/H_2O/(O_2)/N_2$ = 10/12/(5)/30 ml-NTP min^{-1}.

Full line, CH_3OH conversion; dotted line, CO selectivity.

●, in the absence of O_2; ■, in the presence of O_2.

Fig. 6 Oxidative steam reforming of CH_3OH over the Cu/Zn-based catalysts.

Catalyst, 0.2 g; $CH_3OH/H_2O/O_2/N_2$ = 10/12/5/30 ml-NTP min^{-1}; reaction temperature, 200 °C.

Full line, CH_3OH conversion; dotted line, CO selectivity.

●, *hp*-$Cu_{45}/Zn_{45}/Al_{10}$; ■, commercial $Cu/ZnO/Al_2O_3$; ▲, *hp*-Cu_{50}/Zn_{50}; ×, *cp*-Cu_{50}/Zn_{50}.

Fig. 7 TPD profiles of CH_3OH over the *hp*-Cu/Zn/Al catalysts.

(A) M/e = 2, H_2; (B) M/e = 30, HCHO.

Fig. 8 TPD profiles of HCHO over the *hp*-Cu/Zn catalysts.

(A) M/e = 2, H_2; (B) M/e = 28, CO; (C) M/e = 44, CO_2; (D) M/e = 18, H_2O.

Scheme 1.

Reaction mechanism of CH_3OH steam reforming over the Cu catalysts.

Figure 1. K. Takehira et al.

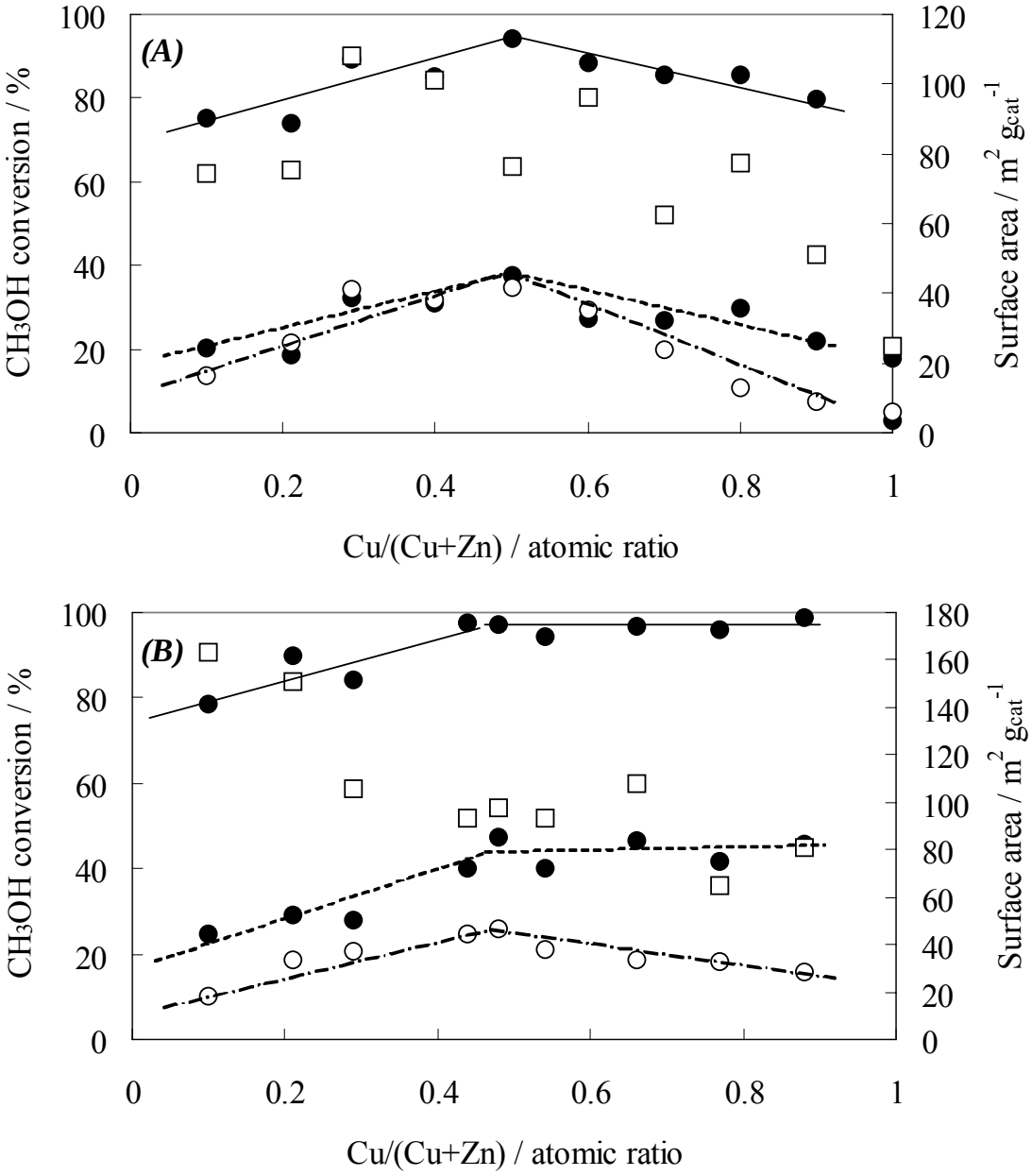

Figure 2. K. Takehira et al.

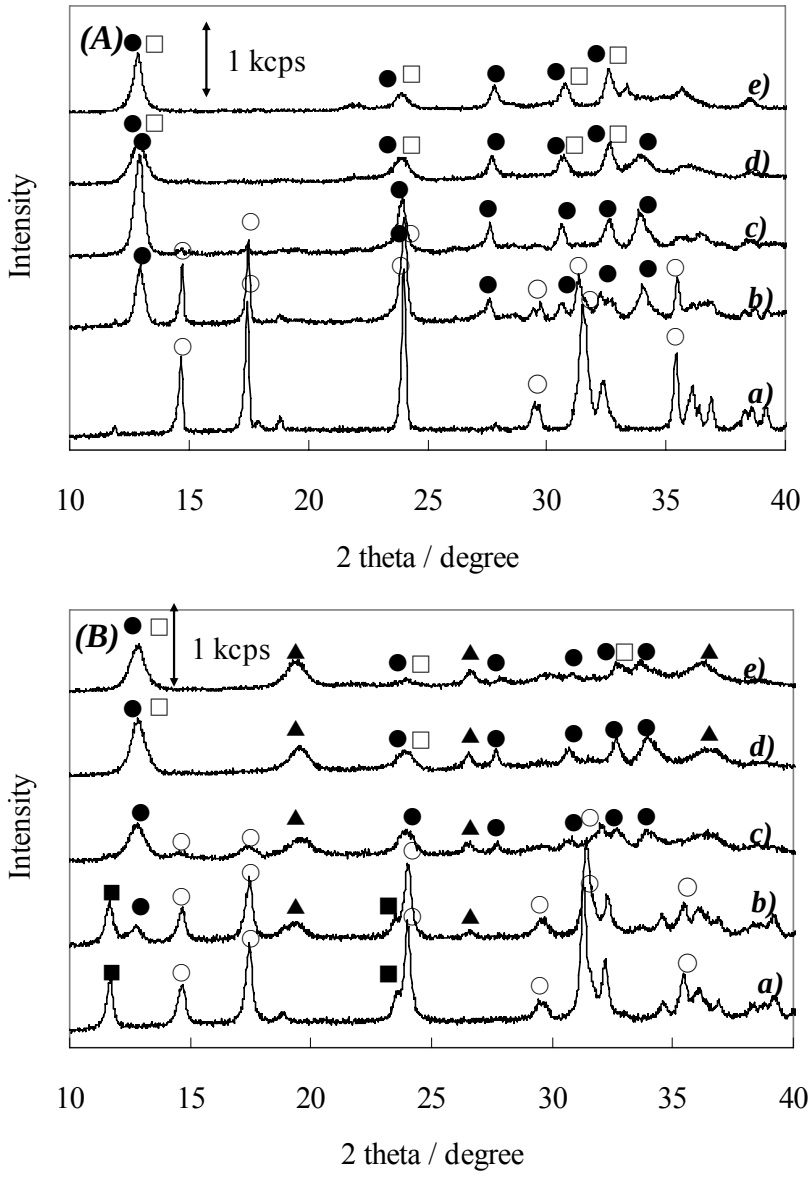

Figure 3. K. Takehira et al.

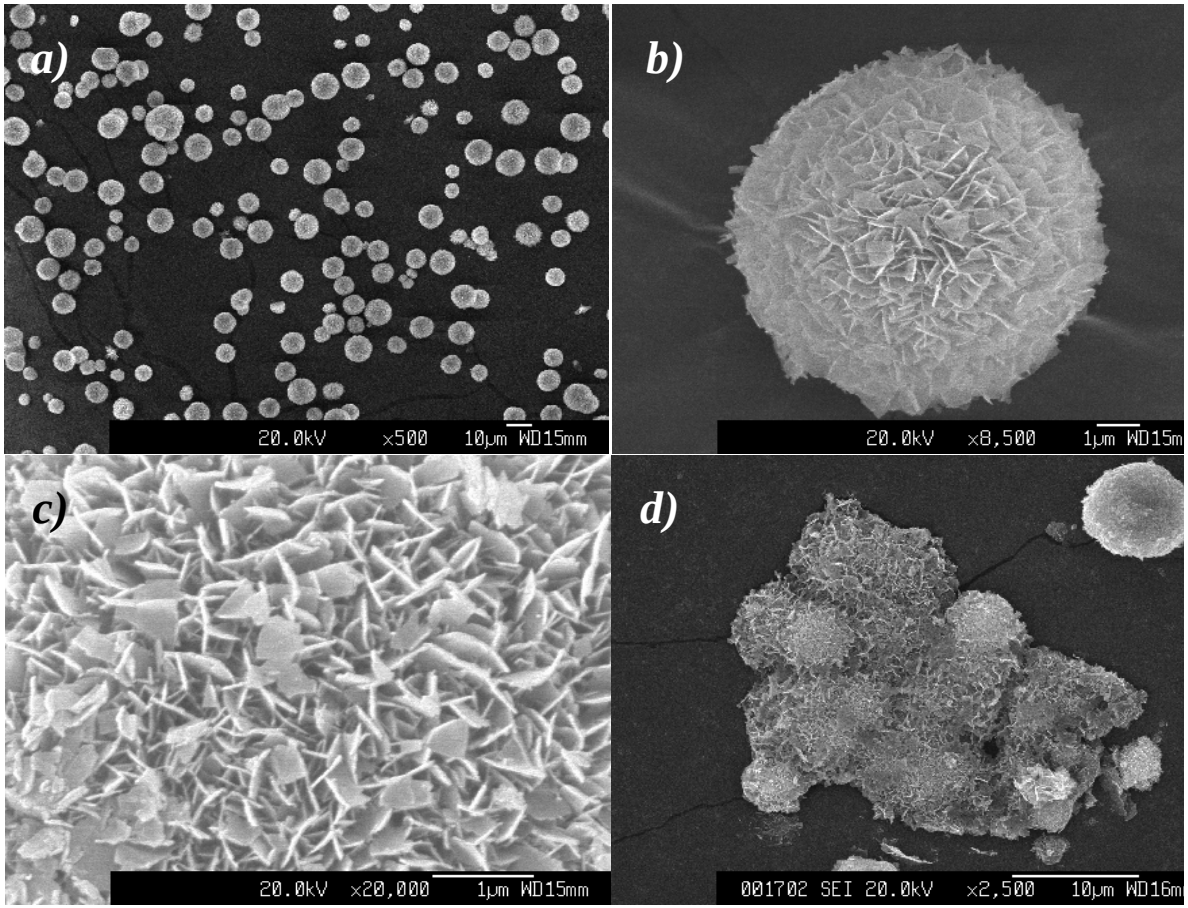

Figure 4. K. Takehira et al.

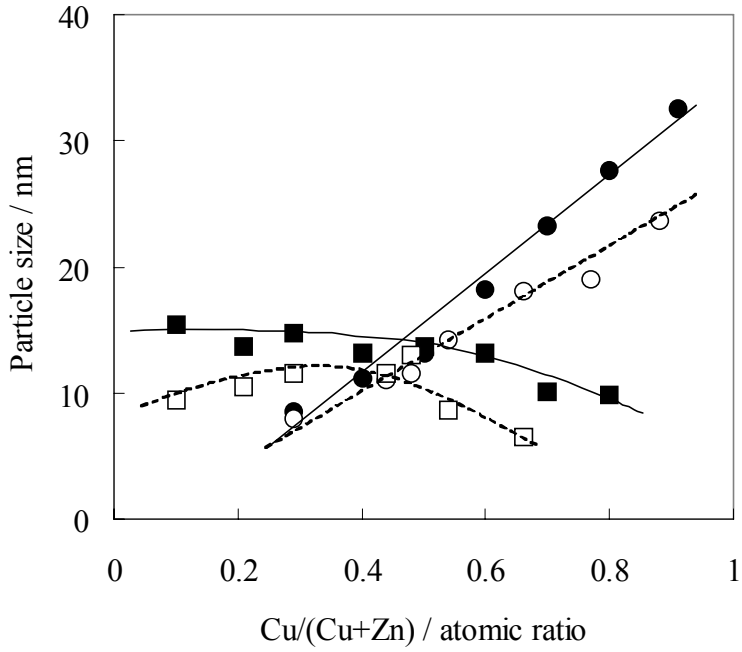

Figure 5. K. Takehira et al.

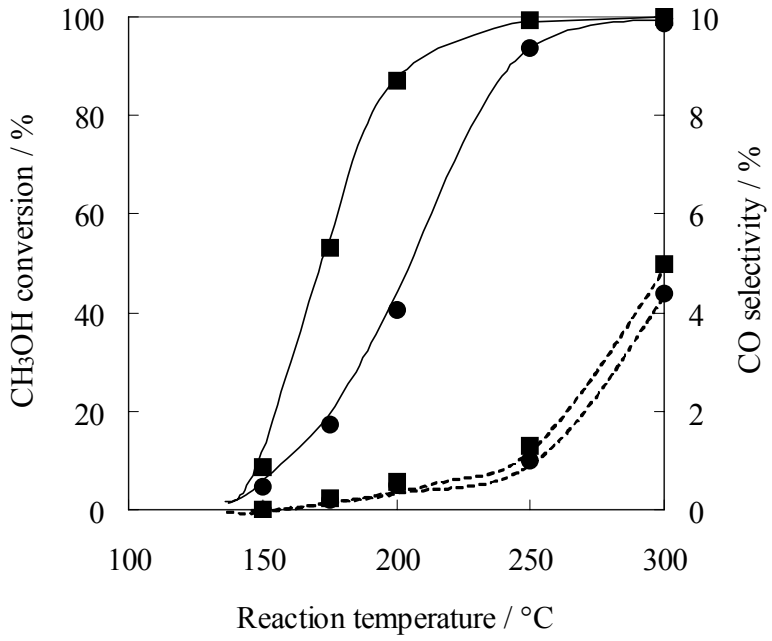

Figure 6. K. Takehira et al.

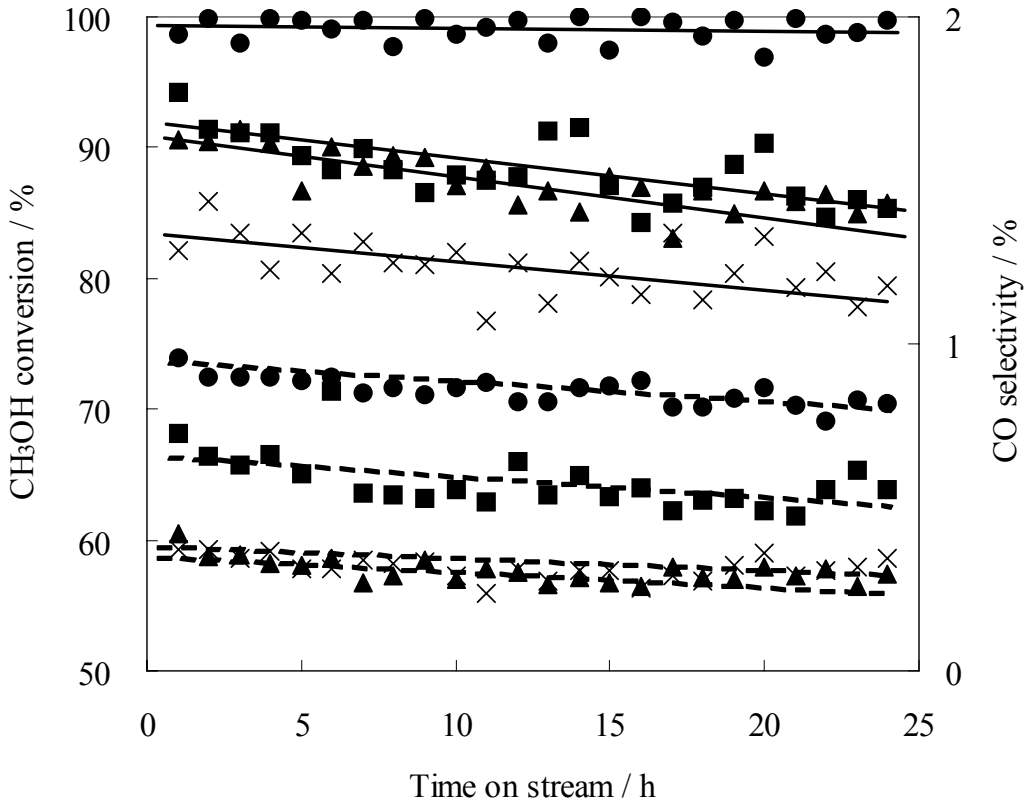

Figure 7. K. Takehira et al.

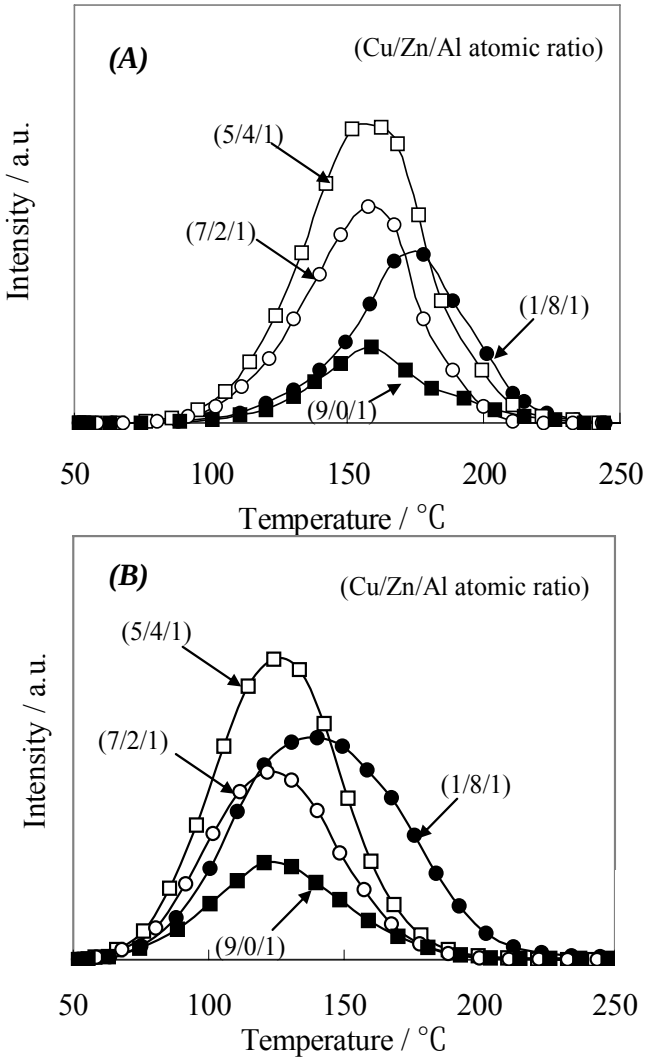

Figure 8. K. Takehira et al.

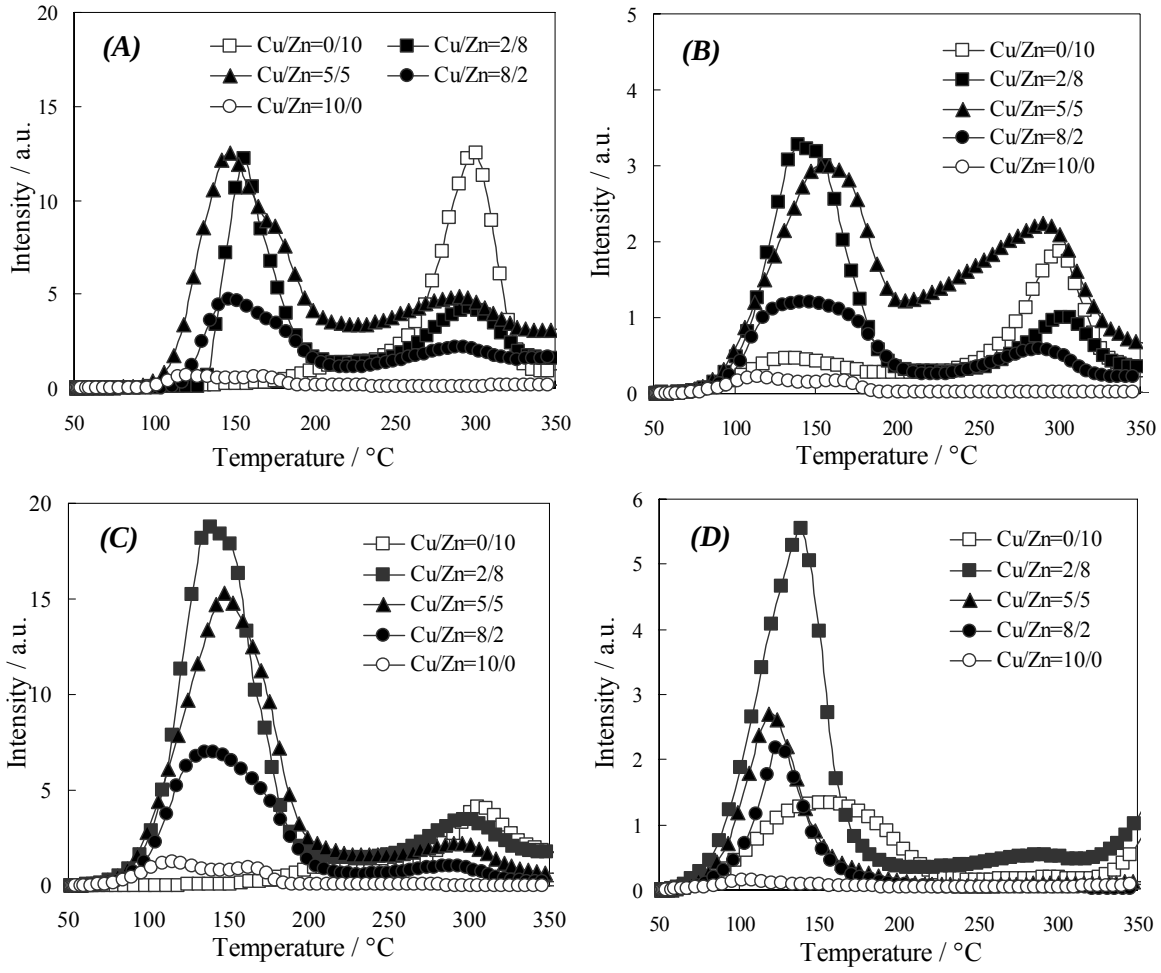

Scheme 1. K. Takehira et al.

Scheme 1

$$CH_3OH \xrightarrow{-H_2} HCHO \xrightarrow{+H_2O,\ -H_2} HCOOH \longrightarrow CO_2 + H_2$$